Records of Natural Products

www.acgpubs.org
ORIGINAL ARTICLE

Exploration of the mechanism of Fuer formula for treating precocious puberty based on transcriptomics and network analysis

Yanli Wang[1], Hao Liu[2], Lili Zhang[3], Wen Tang[3], Han Jiang[1], Lei Gu[1], Sijie Fan[1], Yimin Li[1], Xi Wang[1] and Lili Shang[3*]

[1]The First Clinical Medical College, The First Affiliated Hospital of Anhui University of Chinese Medicine, Hefei 230031, Anhui Province, China
[2]Traditional Chinese Medicine Department, The Second People's Hospital of Anhui Province, Hefei 230031, Anhui Province, China
[3]Department of Pediatrics, The First Affiliated Hospital of Anhui University of Chinese Medicine, Hefei 230031, Anhui Province, China

Abstract: This study investigated the therapeutic mechanism of Fuer Decoction against precocious puberty through transcriptomics and network pharmacology. Female SD rats were allocated to six groups, and an NMA-induced model was established before drug administration. Vaginal opening, estrous cycle, reproductive organ morphology, and serum LH, FSH, E2, and GnRH levels were evaluated. Transcriptome sequencing, differential gene analysis, PPI network construction, GO/KEGG enrichment, and molecular docking were conducted, and NTSR1 was validated via RT-qPCR. UHPLC-MS analysis identified 603 potential active compounds in the decoction. Fuer Decoction alleviated pathological changes and hormonal dysregulation in model rats. NTSR1 emerged as a core target, mainly associated with neuroactive ligand–receptor interactions and calcium signaling pathways. Eicosapentaenoic acid and aurantiamide acetate showed strong binding affinities to NTSR1. These findings suggest that Fuer Decoction may exert therapeutic effects on precocious puberty by modulating these pathways and key genes.

Keywords: Fuer formula, molecular docking, precocious puberty, rats, transcriptomics

Cite this article as:
Wang et al. Exploration of the mechanism of Fuer formula for treating precocious puberty based on transcriptomics and network analysis. (2026). *Records of Natural Products*, 20(2):e25103665

Received: *14 October 2025*
Revised: *10 December 2025*
Accepted: *13 December 2025*
Published: *01 January 2026*

1 Introduction

Precocious puberty (PP) is a frequent endocrine disorder in children, with an annually increasing morbidity worldwide. The distribution of diseases in society has been altered as people's living and social habits, and educational patterns changed during the COVID-19 pandemic, and thus the rate of visits to the doctor for PP and related psycho-behavioral problems in children has increased significantly (Umano et al., 2022). PP refers to the emergence of secondary sex characters in children before the defined age which varies across countries due to differences in age, sex, and region. Usually, the age of the onset of puberty is 2–2.5 standard deviations below the mean for the same sex in the same region (Yu et al., 2024). In China, breast development prior to the age of 7.5 or menarche prior to the age of 10 in girls, and testicular development prior to the age of 9 in boys are the diagnostic criteria for PP currently (Xiong et al., 2023). According to the presence or absence of early initiation of the hypothalamic-pituitary-gonadal axis (HPGA), PP is categorized into peripheral PP (PPP), central PP (CPP), and incomplete PP (IPP) (Park et al., 2021).

Due to an earlier onset of puberty, PP children's development process is accelerated and their bone growth potential is impaired, so their height in adulthood is compromised, and the emergence of secondary sex characters also affects their psychological well-being (Zhang, 2020). Research suggests that PP girls are easily agitated and have great emotional fluctuations, often accompanied by anxiety and irritability (Yang et al., 2020). Moreover, PP children are at higher risk of obesity during adolescence, and they may accumulate more fat and even face a higher risk of cardiovascular disease in adulthood (Dong et al., 2020; Jiang et al., 2023). Gonadotropin-releasing hormone analogs (GnRHa) are currently recommended by clinical guidelines as the first-line drug for PP. However, they may lead to adverse reactions such as rash, allergy, and headache, and they have a long treatment cycle and high cost, restricting their use; they can achieve desired effects only when combined with growth hormones, making some families reluctant to choose this drug (Wu et al., 2023; Zevin & Eugster, 2023). Therefore, it is particularly

*Corresponding Author: Lili Shang.
Email: shanglili188@outlook.com

important to search for new treatment methods and explore new approaches.

In traditional Chinese medicine (TCM), PP belongs to "preceded menorrhea", "breast plague", and "breast nodule". TCM holds that PP is closely related to kidney-liver-spleen relationships. Children often have abundant yang but insufficient yin; if yin-yang disharmony occurs in the kidneys, with fire excess from yin deficiency, children will develop liver-kidney irritation and thus early sexual maturity. Children have good liver function, and if the vital essence in the kidneys is insufficient, kidneys will fail to nourish the liver, and stagnation of liver qi will occur and develop into stagnated fire, causing early sexual maturity. Besides, children also have poor spleen function and disordered spleen-stomach transportation and transformation, so turbid phlegm will be produced in the long run, causing obesity, blockage of qi movement, syndrome of disharmony, and finally early sexual maturity. TCM can delay PP progression through multiple targets and pathways, achieving therapeutic effects, alleviating adverse effects, and ameliorating the quality of life of children with PP (He, 2023). Fuer Formula (FEF) is obtained by adjustment of Zhibai Dihuang Pills from the *Golden Mirror of Medicine*. It is a commonly-used Chinese herbal compound, with Prunella vulgaris (*Prunellae Spic*) and vinegar turtle *(vinegar Trionycis Carapax)* (removing heat from the liver, eliminating stagnation, and nourishing yin) as sovereign drugs, radix geutianae *(Gentiana scabra Bunge)*, chrysanthemum *(Chrysanthemi Flos)*, oriental water plantain *(Alismatis Rhizoma)*, and tree peony bark *(Moutan Cortex)* (clearing heat, removing dampness, and cooling blood) as ministerial drugs, *Lycium chinensis (Lycii Cortex)*, *Scrophularia ningpoensis (Scrophulariae Radix)*, and dried rehmannia root *(Rehmannia glutinosa (Gaetn.) Libosch. ex Fisch. et Mey.)* (nourishing yin to lessen fire) as adjuvant drugs, and malt *(Fructus Hordei Germinatus)* and raw oyster shell *(Ostreae Concha)* (promoting the circulation of qi, and removing stasis) as envoy drugs. FEF is effective for treating PP, but its pharmacodynamic material basis and mechanism have not yet been clarified. Therefore, this study investigated the potential active ingredients, and main targets and pathways of FEF for treating PP by ultra-high performance liquid chromatography-mass spectrometry (UHPLC-MS), network pharmacology, transcriptomics, and experimental validation. The findings are expected to provide a theoretical basis for the clinical application and future research of FEF in PP treatment.

2 Materials and Methods

2.1 Laboratory Animals

Forty-eight female SD rats of SPF grade (21 days old, 80 ± 20 g) were purchased from Henan SCBS Biotechnology Co., Ltd. [Animal Production License No.: SCXK (Henan) 2020-0005]. They were kept in the Laboratory Animal Center of the First Affiliated Hospital of Anhui University of Chinese Medicine at (23 ± 2)°C under (55 ± 5)% relative humidity and 12/12 h light-dark photoperiod, and they had free access to water and food. The Ethics Committee of the First Affiliated Hospital of Anhui University of Chinese Medicine approved all animal experiments (approval No.: AZYFY-2025-1013) in compliance with the National Institutes of Health guidelines for the care and use of laboratory animals.

2.2 Drugs and Reagents

FEF [composed of vinegar turtle *(vinegar Trionycis Carapax)*, *Scrophularia ningpoensis (Scrophulariae Radix)*, *Lycium chinensis (Lycii Cortex)*, radix geutianae *(Gentiana scabra Bunge)*, tree peony bark *(Moutan Cortex)*, oriental water plantain *(Alismatis Rhizoma)*, chrysanthemum *(Chrysanthemi Flos)*, Prunella vulgaris *(Prunellae Spic)*, dried rehmannia root *(Rehmannia glutinosa (Gaetn.) Libosch. ex Fisch. et Mey.)*, raw oyster shell *(Ostreae Concha)*, and malt *(Fructus Hordei Germinatus)*] was provided by the TCM pharmacy of the First Affiliated Hospital of Anhui University of Chinese Medicine; N-methyl-DL-aspartic acid (NMA) (batch No. 220215AD) was provided by Shanghai Aladdin Biochemical Science and Technology Co., Ltd.; xylene (batch No. 10023418), anhydrous ethanol (batch No. 100092683), neutral balsam (batch No. 10004160), and n-butanol (batch No. 100052190) were purchased from China National Pharmaceutical Group Chemical Reagent Co., Ltd.; modified Giemsa staining kit (batch No. G1079-100T), dewaxing solution (eco-friendly) (batch No. G1128), tissue fixative (batch No. G1101), and hematoxylin-eosin (HE) staining kit (batch No. G1076) were purchased from Wuhan Xavier Biotechnology Co., Ltd.; GnRH assay kit (batch No. KS12201), follicle-stimulating hormone (FSH) assay kit (batch No. KS18322), luteinizing hormone (LH) assay kit (batch No. KS11706), and estradiol (E2) assay kit (batch No. KS11525) were purchased from Shanghai Keshun Biotechnology Co., Ltd.; SuperScript™ double-stranded cDNA synthesis kit (batch No. RS-122-2001) and total RNA extraction kit (batch No. 15596026CN) were purchased from Invitrogen, USA; RNA-Seq library prep kit (batch No. RS-122-2001) was purchased from Illumina, USA; EZ-10 spin column total RNA isolation kit (batch No. B618583) was purchased from Sangon Biotech (Shanghai) Co., Ltd.; ABScript™ II qPCR (batch No. RK20403), and 2×SYBR Green qPCR Master Mix II (batch No. RK21203) were purchased from Wuhan ABclonal Biotechnology Co., Ltd.

2.3 Instruments

UHPLC, high-resolution MS, and centrifuge (Thermo Fisher Scientific, USA); balance (Sartorius, Germany); ultrasonic apparatus (Shenzhen Leidebang Electronic Co., Ltd.); homogenizer (Shanghai Jingxin Technology Co., Ltd.); freeze-dryer (Sihuan Furui Keyi Technology Co., Ltd., Beijing); microplate reader (Shandong Fengtou IOT Technology Co. Ltd.); water bath (Shanghai Yiheng Technology Co., Ltd.); paraffin sections, and frozen sections (Wuhan Xavier Biotechnology Co., Ltd.); upright optical microscope imaging system, and imaging system (Nikon, Japan); dehydrator (Diapath S.p.A., Italy); embedder (Wuhan Junjie Electronics Co., Ltd.); microtome (Leica Instruments, Shanghai); tissue flotation workstation (Zhejiang Jinhua Kedi Instrumental Equipment Co., Ltd.);

http://doi.org/10.25135/rnp.2510.3665
Rec. Nat. Prod. 2026, 20(2):e25103665

oven (Tianjin Labotery Instruments Co., Ltd.); freezing microtome (Thermo Fisher Scientific); coverslips (Jiangsu Shitai Experimental Equipment Co., Ltd.); microfluidic chip equipment (Agilent, USA); NanoDrop™ 2000 microspectrophotometer (NanoDrop, USA); Illumina NovaSeq 6000 (Illumina, USA); conventional PCR instrument, and real-time PCR instrument (Bio-Rad, USA); pipette (Eppendorf, Germany).

2.4 UHPLC-MS for composition of FEF

2.4.1 Sample Extraction and Preparation

FEF consists of 10 g of Prunella vulgaris *(Prunellae Spic)*, 10 g of vinegar turtle *(vinegar Trionycis Carapax)*, 10 g of radix geutianae *(Gentiana scabra Bunge)*, 10 g of chrysanthemum *(Chrysanthemi Flos)*, 8 g of *Lycium chinensis (Lycii Cortex)*, 8 g of oriental water plantain *(Alismatis Rhizoma)*, 8 g of *Scrophularia ningpoensis (Scrophulariae Radix)*, 8 g of tree peony bark *(Moutan Cortex)*, 10 g of dried rehmannia root *(Rehmannia glutinosa (Gaetn.) Libosch. ex Fisch. et Mey.)*, 12 g of malt *(Fructus Hordei Germinatus)*, and 15 g of raw oyster shell *(Ostreae Concha)*. TCM decoction pieces were purchased from the TCM pharmacy of the First Affiliated Hospital of Anhui University of Chinese Medicine, and authenticated as genuine by the TCM Teaching and Research Office of the First Affiliated Hospital of Anhui University of Chinese Medicine. First, the decoction piece of FEF crude drug was added with 10-fold volumes of water and soaked for 45 min. After boiling vigorously, it was simmered for 40 min and filtered for the first time. Then the filtrate was added with 8-fold volumes of water, and after boiling vigorously, it was simmered for 30 min and filtered again. The two filtrates were merged, concentrated, and cryopreserved. After thawing, the liquid sample was centrifuged (12,000 rpm, 15 min), and the supernatant (300 μL) was aspirated, added with extracting buffer (1,000 μL, methanol: acetonitrile: water = 2:2:1, with an isotope-labeled internal standard), mixed by vortexing for 30 s, and sonicated for 5 min in an ice water bath. Then the sample was stored in a refrigerator at −20°C for 1 h, followed by centrifugation (12,000 rpm, 15 min). Finally, the supernatant was aspirated and filtered through a 0.22 μM membrane into an injection vial for later tests.

2.4.2 Detection Conditions

Using UPLC, the sample was separated on a Phenomenex Kinetex C18 column (2.1 × 100 mm, 2.6 μM), with a 0.01% acetic acid-contained aqueous phase as the A-phase, and isopropanol: acetonitrile (1:1, v/v) as the B-phase. The injection volume was 2 μL, and the sample plate temperature was 4°C.

2.4.3 Mass Spectrometey

MS was performed on samples in the positive and negative ion modes, using the following parameters: electrospray voltage (3.8 kV and −3.4 kV for the positive and negative ion modes), capillary temperature (320°C), collision energy (SNCE 20/30/40), full spectral resolution (60,000), and MS/MS resolution (15,000).

2.4.4 Data Processing

After tests, the raw data were converted by ProteoWizard into mzXML format, and metabolites were identified by the self-developed R package using Biotree TCM (v1.0) and BT-HERB (v1.0). The results were visualized (Doppler et al., 2016; Wang et al., 2016). The identification of Chinese herbal medicinal ingredients was carried out following the substance identification grading standards published by the internationally recognized body for food standard-setting (Sumner et al., 2007; Zhou et al., 2022): Level 1 (Identification Grade), Level 2 (Annotation Grade), Level 3 (Category Annotation Grade), and Level 4 (Unknown). Biotree TCM (V 1.0) is a self-built database of reference standards for herbal ingredients, containing second-order spectra and retention time data for over 5,000 compounds derived from TCM, which can provide the highest level (Level 1) of precise structural identification for unknown spectra. BT-HERB (V 1.0) is a public spectral database of herbal ingredients, containing over 15,000 compounds derived from TCM, which can provide a suboptimal level (Level 2) of structural annotation for unknown spectra. The two databases encompass characteristic ingredients, including phenylpropanoids, terpenoids, and alkaloids of over 5,000 representative Chinese medical herbs. They cover a wide range of sources and structural types of TCM, providing a comprehensive basis of characterization for the identification of Chinese herbal medicinal ingredients.

2.5 Animal Experiments

2.5.1 Grouping, Modeling, and Drug Administration

Forty-eight female SD rats (21 days old) were randomized into normal control (CON) group, PP group, triptorelin group, high-dose FEF (HD) group, medium-dose FEF (MD) group, and low-dose FEF (LD) group, with eight in each group. To minimize potential confounders, rats were randomly assigned to different cages to reduce the influence of the cage effect. The laboratory staff was responsible for the assignment process and was not aware of the grouping. All rats were acclimated for 5 days. From Day 26, rats in each group except the CON group were injected subcutaneously with NMA (40 mg·kg^{-1}) at 2:00 p.m. and 4:00 p.m. daily to induce the PP model (Yu & Zhang, 2023), while saline of the same volume was given in the CON group. The rats in the PP group were observed daily for the status of vaginal opening. When we observed that the vagina opened, the injection of NMA was terminated in each group at 1:1 except the CON group (the injection of saline was terminated).

Clinical studies suggest that the usual daily dose of FEF in adults is 109 g of crude drug. According to the clinical dose conversion between laboratory animals and human beings in *Experimental Methodology of Pharmacology*, when converted to the body surface area, the equivalent clinical daily dose in rats is approximately 24.2 g/kg (equivalent to approximately 6.3 times the human dose based on body weight) (Wei et al., 2010). Therefore, we set up HD (48.4 g/kg/d), MD (24.2 g/kg/d), and LD (12.1 g/kg/d) FEF groups, corresponding to 2 times, 1 times, and 0.5 times the clinical equivalent

dose. In this way, we can ensure that even the maximum dose is only 2 times the clinical equivalent dose, falling within the safe dose range for animal experiments. Then with a dose volume of 10 mL/kg, FEF was prepared into fresh decoction at crude drug concentrations of 4.84 g/mL, 2.42 g/mL, and 1.21 g/mL, respectively, for gavage. Triptorelin 100 μg/kg was subcutaneously injected in the triptorelin group, and saline of the same volume was given in the CON group and PP group.

2.5.2 Sampling

The status of vaginal opening was observed and recorded at 8:00 a.m. every day. When we observed that the vagina opened in the PP group, the vaginal smears prepared were examined daily under a microscope to determine the estrous cycle. Following one estrous cycle, the rats were sacrificed in the dioestrus phase in each group at 1:1. Three to five min after successful anesthesia with intraperitoneal injection of 3% pentobarbital sodium solution (0.04 g/kg), abdominal aortic blood was drawn and left to stand at room temperature for 1 h, followed by centrifugation. The separated serum was placed in sterile EP tubes for later use. After blood sampling, the uterine tissue was located, upward along which the ovaries were found, and the uterus and ovaries were removed. A portion of the uterine and ovarian tissues was fixed and embedded in paraffin, and the sections underwent histopathological examination. The other portion of the ovarian tissues was stored at −80°C for transcriptome sequencing and fluorescence RT-qPCR.

2.5.3 Morphologic Observation of Uterine and Ovarian Tissues

The uterine and ovarian tissues were harvested, soaked in 10% formalin for 24 h, fixed in 4% paraformaldehyde aqueous solution, and embedded in paraffin. The sections were then deparaffinized, stained by HE, and mounted with neutral balsam, followed by morphologic observation and image acquisition of uterine and ovarian tissues under a light microscope.

2.5.4 Detection of Biochemical Indicators

The levels of E2, FSH, LH, and GnRH were detected by ELISA following the kit instructions, involving standard dilution and sample loading, incubation, washing, color development, and termination of the reaction. With zeroing by blank wells, we measured the absorbance at 450 nM of each well. Based on the standard curve of the standard, the corresponding levels were calculated.

2.6 Screening of Potential Active Ingredients and Related Targets of FEF

With the TCM name (FEF) as the keyword, the chemical ingredients of Prunella vulgaris *(Prunellae Spica)*, chrysanthemum *(Chrysanthemi Flos)*, oriental water plantain *(Alismatis Rhizoma)*, *Lycium chinensis (Lycii Cortex)*, *Scrophularia ningpoensis (Scrophulariae Radix)*, malt *(Fructus Hordei Germinatus)*, radix geutianae *(Gentiana scabra Bunge)*, and tree peony bark *(Moutan Cortex)* were searched in TCMSP (http://www.tcmsp-e.com), from which potential active ingredients (drug likeness ≥ 0.18 and oral bioavailability ≥ 30%) were screened. The potential active ingredients and targets of dried rehmannia root *(Rehmannia glutinosa (Gaetn.) Libosch. ex Fisch. et Mey.)*, raw oyster shell *(Ostreae Concha)*, and vinegar turtle *(vinegar Trionycis Carapax)* were screened (adjusted P-value < 0.05) in BATMAN-TCM (http://bionet.ncpsb.org/batman-tcm/). In addition, the CAS number of potential active ingredients was converted into SMILES (PubChem), and then the relevant targets were searched in Swiss Target Prediction (www.swisstargetprediction.ch/index.php) and TargetNet (http://targetnet.scbdd.com/). The targets were annotated and corrected in the UniProt, with "Reviewed" and "Human" targets screened.

2.7 Transcriptome Sequencing

The frozen ovarian tissues were taken, and three biological replicates were selected in each group for quality control. mRNA was extracted and ribosomal RNA was removed to construct strand-specific libraries and small RNA libraries. These libraries were subjected to double-ended sequencing on a high-throughput sequencing platform. To obtain clean reads for data analysis, the raw reads were first filtered. The resulting high-quality sequences were aligned to the specified reference genome, and according to the alignment results, the gene expression was calculated. Transcriptome sequencing and upstream analysis were performed with the assistance of Hefei Deerpu Biotechnology Co., Ltd.

We performed differential expression analyses on the transcriptome sequencing data, and a statistical model based on negative binomial distribution was established using DESeq2 software to calculate the log2 fold change of gene expression and its statistical significance. Following the pre-established criteria ($|\log2FoldChange| > 1$ and $P < 0.05$), the differentially expressed genes (DEGs) were systematically screened in three important pairs: CON *vs*. PP, PP *vs*. HD/MD/LD, and HD/MD/LD *vs*. triptorelin. Finally, biologically significant DEGs were obtained.

Using the ggvenn package, a Venn diagram was created to visualize the intersection of DEGs (CON *vs*. PP, PP *vs*. HD/MD/LD, and HD/MD/LD *vs*. triptorelin) with the drug targets, from which the core candidate genes in FEF for treating CPP were screened. Cross-species homologous gene conversion was conducted in the UniProt to obtain the standardized human gene nomenclature.

2.8 Protein-Protein Interaction (PPI) and Functional Enrichment Analyses of Core Target

The PPI network of the core target NTSR1 was constructed using the STRING database (species: *Homo sapiens*, confidence > 0.15). Core adjacent proteins of NTSR1 were screened and identified, followed by network visualization. Besides, Gene Ontology (GO) (biological process BP, molecular function MF, cellular component CC), and Kyoto Encyclopedia of Genes and Genomes (KEGG)

http://doi.org/10.25135/rnp.2510.3665
Rec. Nat. Prod. 2026, 20(2):e25103665

pathway enrichment analyses were performed using the ClusterProfiler package (v4.14.3), with a threshold of $P < 0.05$. Enrichment results were visualized using the enrichplot package.

2.9 Molecular Docking

Molecular docking was conducted between key potential active ingredients screened above and core target NTSR1, as follows: 1) The 3D structures of the active ingredients were downloaded from the PubChem, saved in SDF format and transformed into PDB format by PyMOL. 2) The protein crystal structure of NTSR1 was obtained from the PDB (PDB code: 6UP7 (Huang et al., 2020)). 3) The active ingredients and target protein were preprocessed using AutoDock Tools (to remove original ligands and water molecules, add hydrogen atoms and charges, and convert to PDBQT format). 4) Molecular docking was performed with AutoDock Vina, and the active pocket was defined based on the original ligand binding site in the PDB structure (center coordinates: X = 123.65, Y = 106.64, Z = 116.131; pocket dimension: 25.066 Å × 25.066 Å × 25.066 Å), with all other parameters set to default values. 5) The optimal docking conformation (with the lowest binding energy) was visualized using PyMOL.

2.10 RT-qPCR Validation for mRNA Expression in Key Targets

RT-qPCR validation was conducted on the key target NTSR1. Total RNA was extracted from the ovarian tissues for quality control strictly following the kit instructions, and it was reversely transcribed using the RT kit and amplified using the amplification PCR kit. The gene expression was calculated using the $2^{-\triangle\triangle Ct}$ method, and the primer sequences used are shown in Table S1.

2.11 Statistical Analysis

The independent statistics personnel were responsible for data analysis and were not aware of the animal grouping. SPSS27.0 software was utilized for statistical analyses. Measurement data were presented by mean ± standard deviation ($\bar{\chi} \pm s$). Normally distributed measurement data with homogeneous variance were compared among groups by one-way ANOVA, while those with heterogeneous variance

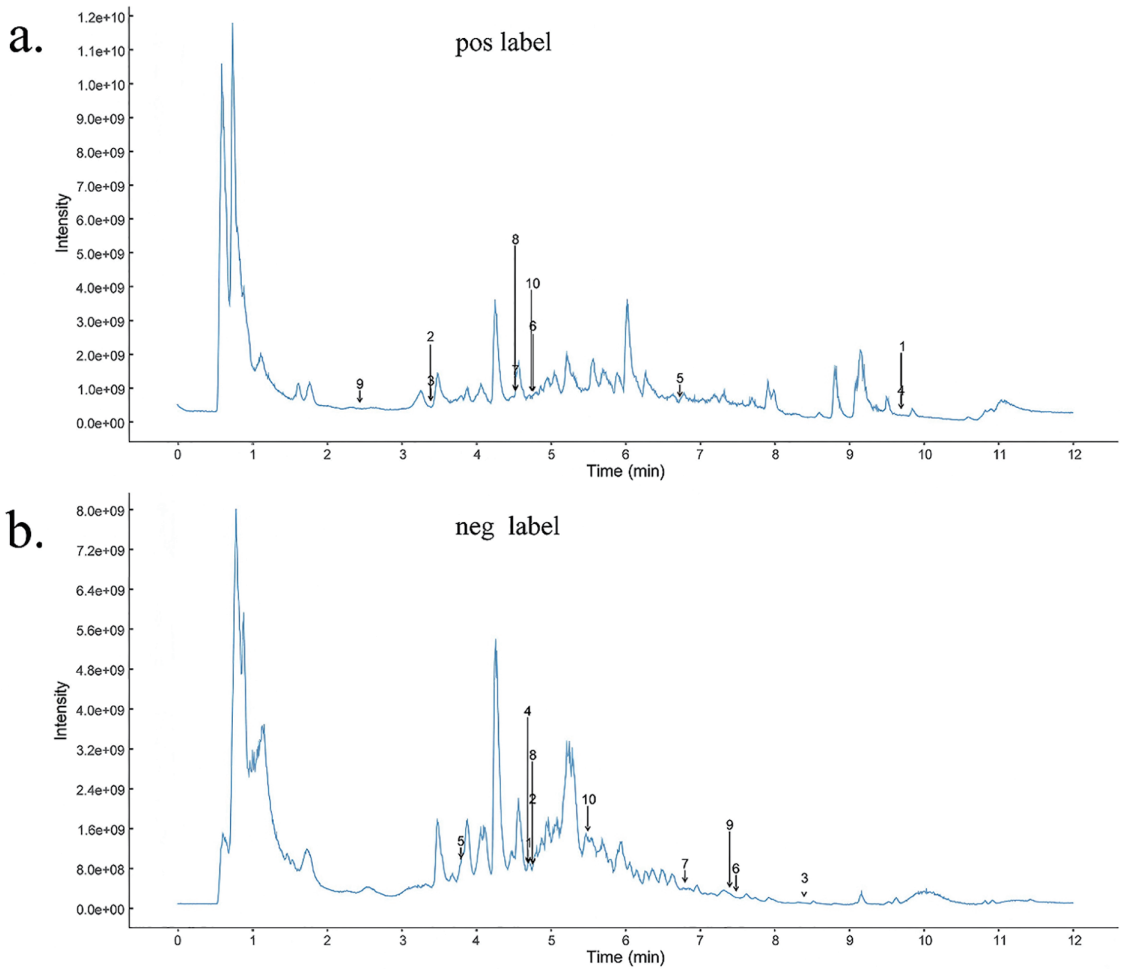

Figure 1. The total ion chromatograms (TICs) of FEF in the positive and negative ion modes. Abbreviations: pos label: positive label neg label: negative label

Table 1. TIC peak in positive ion mode

No.	Compound name	Molecular formula	Mass-to-charge ratio (m/z)	Retention time (rt)
1	Naringin	C27H32O14	581.1869	299.4
2	Tagatose	C6H12O6	203.053	44.6
3	Allose	C6H12O6	203.053	44.6
4	7-[4,5-dihydroxy-6-(hydroxymethyl)-3-[(2S,3R,4R,5R,6S)-3,4,5-trihydroxy-6-methyl-tetrahydropyran-2-yl]oxy-tetrahydropyran-2-yl]oxy-5-hydroxy-2-(4-hydroxyphenyl)chroman-4-one	C27H32O14	581.1869	299.4
5	Nobiletin	C21H22O8	403.1393	380.9
6	(2*Z*)-6-hydroxy-2-[(4-hydroxy-3-methoxy-phenyl)methylene]benzofuran-3-one	C16H12O5	285.0761	360.4
7	Sulfuretin	C15H10O5	271.0605	341.8
8	7,3′,4′-Trihydroxyflavone	C15H10O5	271.0605	341.8
9	Indole-3-carboxaldehyde	C9H7NO	146.0602	317.4
10	Guanosine	C10H13N5O5	284.0995	103.9

Table 2. TIC peak in negative ion mode

No.	Compound name	Molecular formula	Mass-to-charge ratio (m/z)	Retention time (rt)
1	Oleic acid	C18H34O2	281.2484	571.9
2	Kaempferol	C15H10O6	285.0402	374.6
3	(1R,2R,4aS,6aS,6bR,10R,11S,12R,12aR)-1,10,11,12-tetrahydroxy-1,2,6a,6b,9,9,12a-heptamethyl-2,3,4,5,6,6a,7,8,8a,10,11,12,13,14b-tetradecahydropicene-4a-carboxylic acid	C30H48O6	503.3375	432.1
4	*trans*-Vaccenic acid	C18H34O2	281.2484	571.9
5	Myristic acid	C14H28O2	227.2015	545.3
6	Glycodeoxycholic acid	C26H43NO5	448.3065	497.5
7	Allocholic acid	C24H40O5	407.2797	434.9
8	1,3,5,6-tetrahydroxy-2-methyl-anthracene-9,10-dione	C15H10O6	285.0402	424.6
9	Aurantiamide acetate	C27H28N2O4	443.1972	422.9
10	(*Z*)-9,10,11-trihydroxyoctadec-12-enoic acid	C18H34O5	329.2331	414.1

were compared by non-parametric tests. $P < 0.05$ was deemed statistically significant.

3 Results

3.1 FEF Composition

The total ion chromatograms (TICs) of FEF in the positive and negative ion modes are displayed in Figure 1. We finally identified 603 compounds by the primary and secondary MS data, and the top 10 compounds in each mode were selected as examples for TIC peak picking (Tables 1 and 2).

3.2 Vaginal Opening Time and Estrous Cycle

A total of 48 rats met the eligibility criteria and were included. The time of vaginal opening was recorded in each group to reflect the PP modeling results. The vagina opened much earlier in the PP and LD groups than in the CON group; it opened much later in the triptorelin, HD, and MD groups than in the PP group, all displaying statistically significant differences ($P < 0.01$) (Figure 2).

The vaginal exfoliated cell smear in the PP group was observed under a light microscope to determine the estrous cycle. Nuclear epithelial cells were dominant in the pro-oestrus phase; rosy-red, non-nucleated keratinized cells were dominant in the oestrus phase; the meta-oestrus phase was characterized by the withdrawal of estrogen and the thinning of the epithelial layer, with an equal number of nuclear epithelial cells, keratinized cells, and leukocytes; in the dioestrus phase, also known as the stationary phase, leukocyte infiltration began (Figure 3).

3.3 Morphology of Uterine and Ovarian Tissues in Each Group

As observed by HE staining, as compared to the CON group, the uterus of rats became larger, the endometrial thickness increased significantly, and many glands and cuboidal or columnar mucosal epithelium could be observed in the PP group; compared with the PP group, the triptorelin, HD, MD, and LD groups had fewer uterine glands, decreased

http://doi.org/10.25135/rnp.2510.3665
Rec. Nat. Prod. 2026, 20(2):e25103665

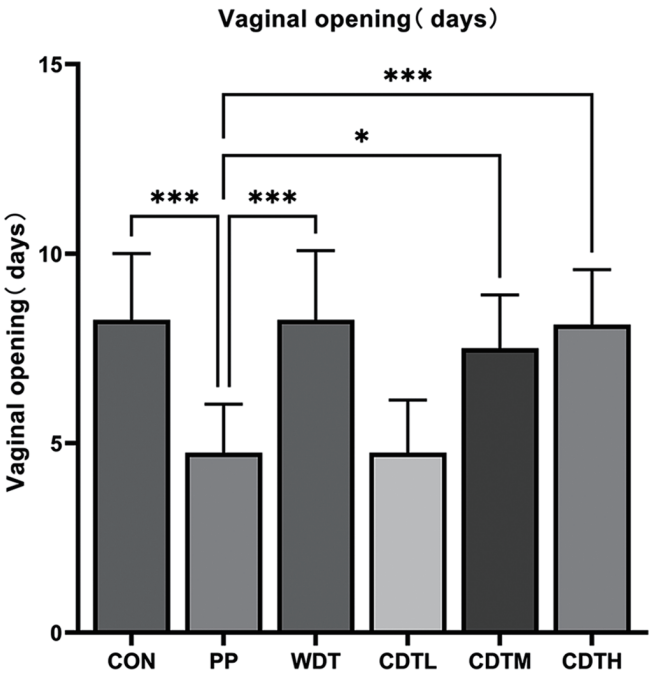

Figure 2. The time of vaginal opening was recorded in each group to reflect the PP modeling results. Abbreviations: PP: Model groups

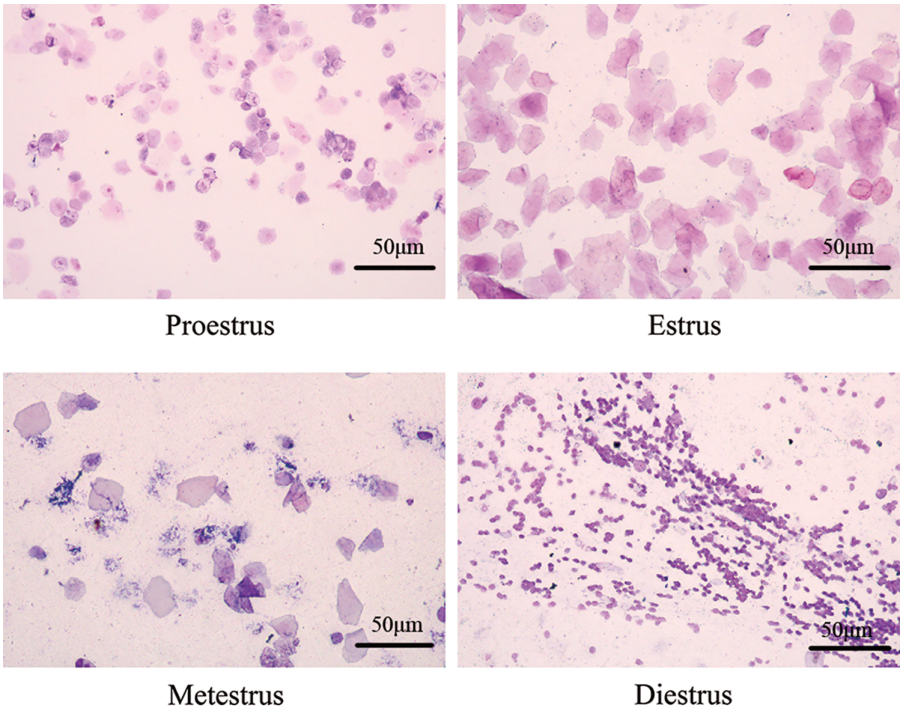

Figure 3. The estrous cycle in the model group was determined by vaginal cytology smears

endometrial thickness, and single-layer columnar mucosal epithelium (Figure 4).

The results of HE staining of ovarian tissues showed that the PP group had follicles at all levels, dominated by primordial follicles, and a small number of mature follicles, atretic follicles, and corpus luteum as compared to the CON group. Compared with the PP group, the triptorelin, HD, MD, and LD groups had fewer mature and atretic follicles, a larger number of secondary follicles, significantly less corpus luteum, and fewer follicles (Figure 5).

3.4 Serum Hormone Levels in Each Group

The PP group had far higher levels of serum LH, FSH, E2, and GnRH than the CON group ($P < 0.01$); the HD, MD,

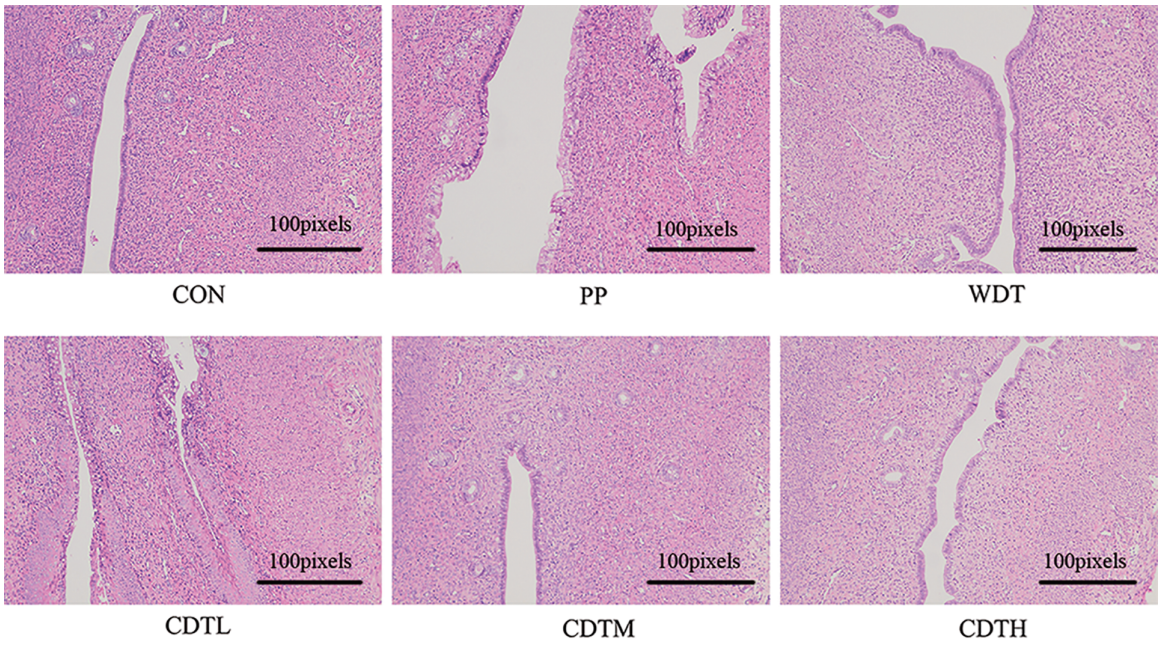

Figure 4. Evaluation of uterine volume and endometrial thickness via H&E staining. Uterine volume and endometrial thickness were assessed across the control (CON), model (PP), triptorelin (WDT), and low-/medium-/high-dose TCM (CDTL/CDTM/CDTH) groups using hematoxylin–eosin (H&E)-stained sections

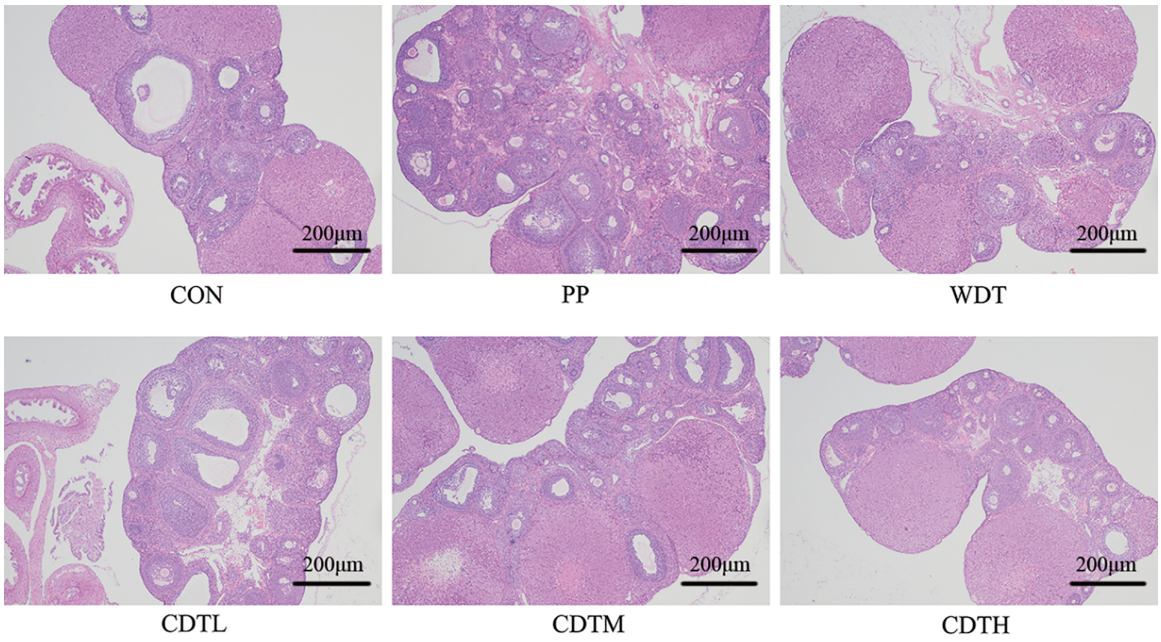

Figure 5. Hematoxylin–eosin (H&E) staining of ovarian tissues across groups. Ovarian tissues from the control (CON), model (PP), triptorelin (WDT), and low-/medium-/high-dose TCM (CDTL/CDTM/CDTH) groups were stained with H&E

and triptorelin groups had far lower levels than the PP group (*$P < 0.05$, **$P < 0.01$) (Figure 6).

3.5 Potential Targets and Related Targets of FEF

A total of 171 potential active ingredients were searched from the database, including 11 for Prunella vulgaris *(Prunellae Spic)*, 20 for chrysanthemum *(Chrysanthemi Flos)*, 13 for *Lycium chinensis (Lycii Cortex)*, 10 for oriental water plantain *(Alismatis Rhizoma)*, 9 for *Scrophularia ningpoensis (Scrophulariae Radix)*, 11 for tree peony bark *(Moutan Cortex)*, 18 for malt *(Fructus Hordei Germinatus)*, 10 for radix gentianae *(Gentiana scabra Bunge)*, 23 for dried rehmannia root *(Rehmannia glutinosa (Gaetn.) Libosch. ex Fisch. et Mey.)*, 18 for raw oyster shell *(Ostreae Concha)*, and 28 for vinegar turtle *(vinegar Trionycis Carapax)*. Following standardization in the UniProt, 11,796 targets were obtained. After duplicate

http://doi.org/10.25135/rnp.2510.3665
Rec. Nat. Prod. 2026, 20(2):e25103665

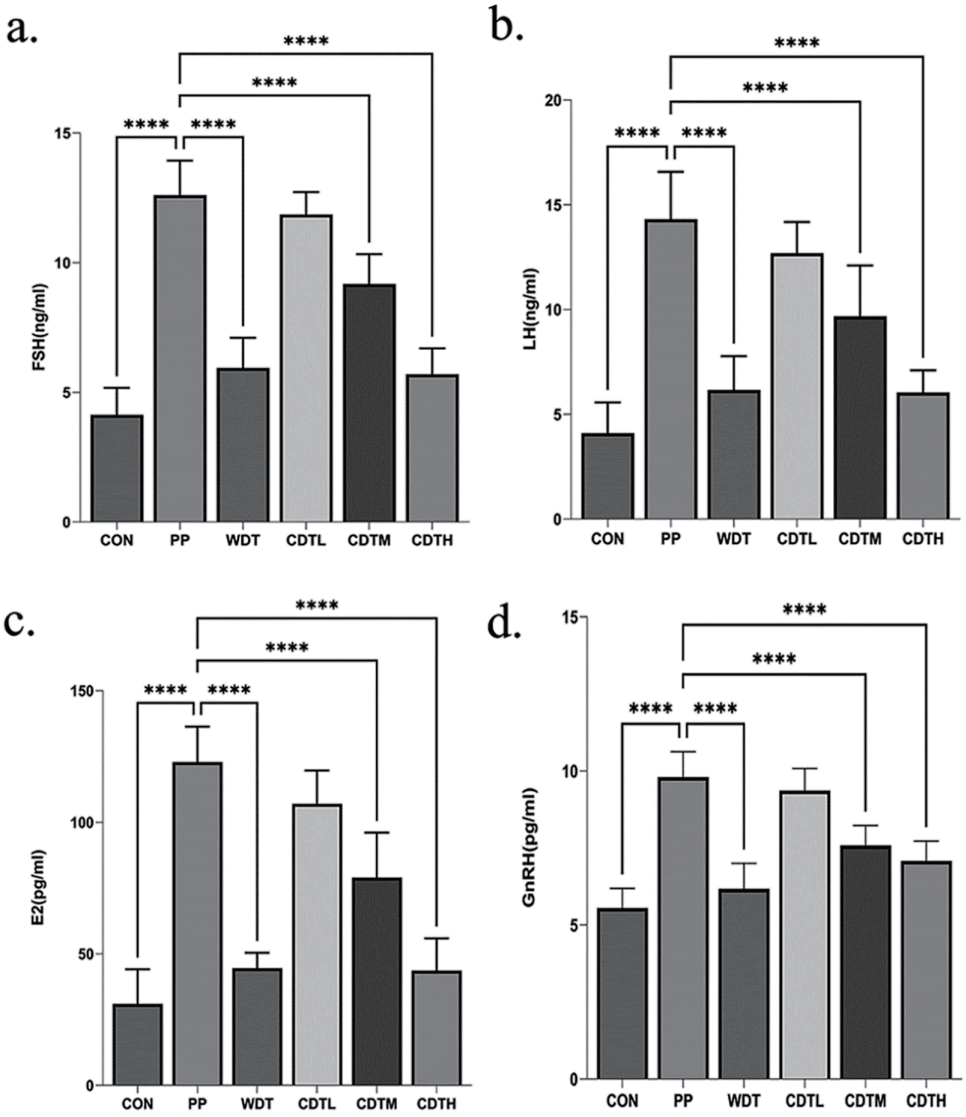

Figure 6. Comparison of LH, FSH, E2, and GnRH among tthe control (CON), model (PP), triptorelin (WDT), and low-/medium-/high-dose TCM (CDTL/CDTM/CDTH) groups

removal, 1,332 targets were finally obtained. The number of potential active ingredients and corresponding targets is shown in Table 3, and the specific names of potential active ingredients are listed in Table S2.

3.6 DEGs Screened

According to the transcriptome sequencing results, we screened 256 DEGs (189 up-regulated and 67 down-regulated) in the PP *vs.* CON group, 88 DEGs (53 up-regulated and 35 down-regulated) in the PP *vs.* HD/MD/LD groups, and 2,447 DEGs (321 up-regulated and 2,126 down-regulated) in the HD/MD/LD *vs.* triptorelin group. The volcano plot, heatmap, and statistical number are displayed in Figure 7. We further identified four intersecting genes (CYP4F4, PLA2G4C, NTSR1, and OLFM2) as the signature DEGs for PP treatment with FEF. Then the four genes were intersected with the active ingredient targets screened in 3.5 to obtain the key target NTSR1 (Figure 8).

3.7 PPI and Functional Enrichment Analyses of NTSR1

To further investigate the molecular regulatory mechanism of NTSR1, its PPI network was constructed using the STRING database to identify core adjacent proteins of NTSR1 (Figure 9a). The GO functional enrichment analysis revealed that the DEGs were mainly enriched in the neuropeptide, phosphatidylinositol-activated G protein-coupled receptor, and neurotrophic factor signaling pathways (BP); they were mainly enriched in the cytoplasmic components of the outer membrane, dense core vesicles, and outer segments of the photoreceptors (CC); they were mainly enriched in the G protein-coupled receptor, neurotrophic factor receptor binding, and neuropeptide receptor activity (MF) (Figure 9b). Besides, the KEGG pathway enrichment analysis revealed that the DEGs were mainly involved in key pathways closely related to the pathogenesis of PP and TCM intervention, such as neuroactive ligand-receptor interaction,

Table 3. Potential active ingredients in traditional Chinese botanical drugs and their associated therapeutic targets

Traditional Chinese botanical drugs	Active ingredient (types)	Therapeutic targets
Prunella vulgaris (*Prunella Sp.*)	11	1251
Chrysanthemum (*Chrysanthemi Flos*)	20	2591
Lycium chinensis (*Lycii Cortex*)	13	1249
Oriental water plantain (*Alismatis Rhizoma*)	10	713
Scrophularia ningpoensis (*Scrophulariae Radix*)	9	294
Tree peony bark (*Moutan Cortex*)	11	852
Malt (*Fructus Hordei Germinatus*)	18	1027
Radix geutianae (*Gentiana scabra Bunge*)	10	802
Dried rehmannia root (*Rehmannia glutinosa (Gaetn.) Libosch. ex Fisch. et Mey.*)	23	1219
Raw oyster shell (*Ostreae Concha*)	18	934
Vinegar turtle (*vinegar Trionycis Carapax*)	28	837

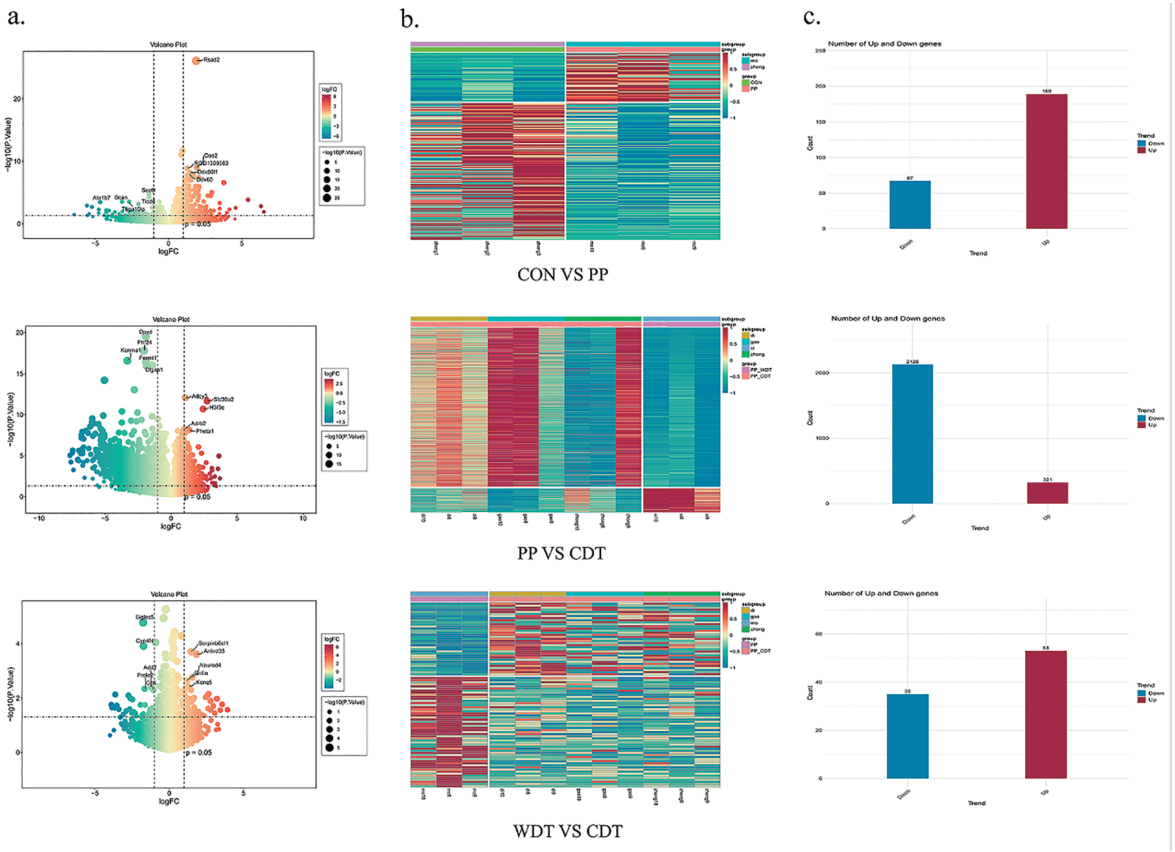

Figure 7. Differentially expressed genes (DEGs) among groups. Transcriptome sequencing identified: (a) 256 DEGs (189 up-, 67 down-regulated) in PP *vs.* CON; (b) 88 DEGs (53 up-, 35 down-regulated) in PP *vs.* HD/MD/LD; (c) 2,447 DEGs (321 up-, 2,126 down-regulated) in HD/MD/LD *vs.* triptorelin. Volcano plots, heatmaps, and DEG count statistics are shown. Abbreviations: CON: the control groups PP: Model groups; WDT: triptorelin groups; CDTL/CDTM/CDTH: low-/medium-/high-dose TCM groups

dopamine synapse, calcium, and hormone signaling pathways (Figure 9c). Furthermore, to systematically elucidate the specificity of TCM intervention in pathway regulation, separate enrichment analyses were performed on the upregulated DEGs and downregulated DEGs identified between the PP group and the TCM group (CDT group). The results showed that up-regulated DEGs were primarily enriched in lipid and cholesterol metabolism pathways and immune function-related pathways, and down-regulated DEGs were primarily enriched in glucose metabolism pathways, some exocrine function-related pathways, and fatty acid metabolism pathways. This suggests that FEF may achieve therapeutic effects by bidirectional regulation of metabolism and immune-related pathways (Figure 10).

http://doi.org/10.25135/rnp.2510.3665
Rec. Nat. Prod. 2026, 20(2):e25103665

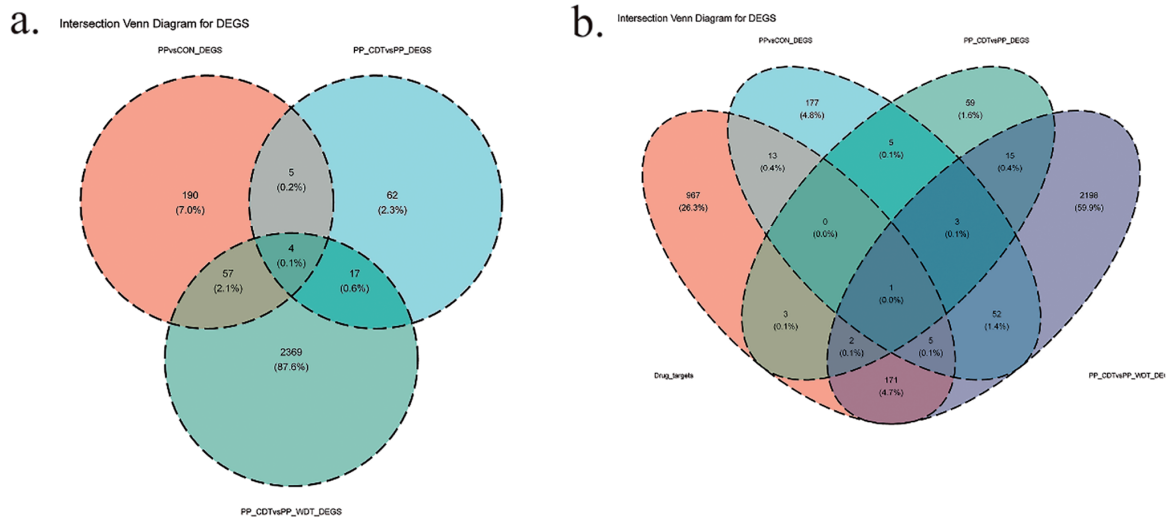

Figure 8. Identification of key target for PP treatment with FEF. Four signature DEGs (CYP4F4, PLA2G4C, NTSR1, OLFM2) were identified in PP; intersection with FEF active ingredient targets (Section 3.5) yielded the key target NTSR1. Abbreviations: PP *vs.* CON: Model groups *vs.* Control groups; PP_CDT *vs.* PP: TCM groups *vs.* Model groups; PP_CDT *vs.* PP_WDT: TCM groups *vs.* triptorelin groups; Drugs _Targets: Potential active targets of traditional Chinese medicine

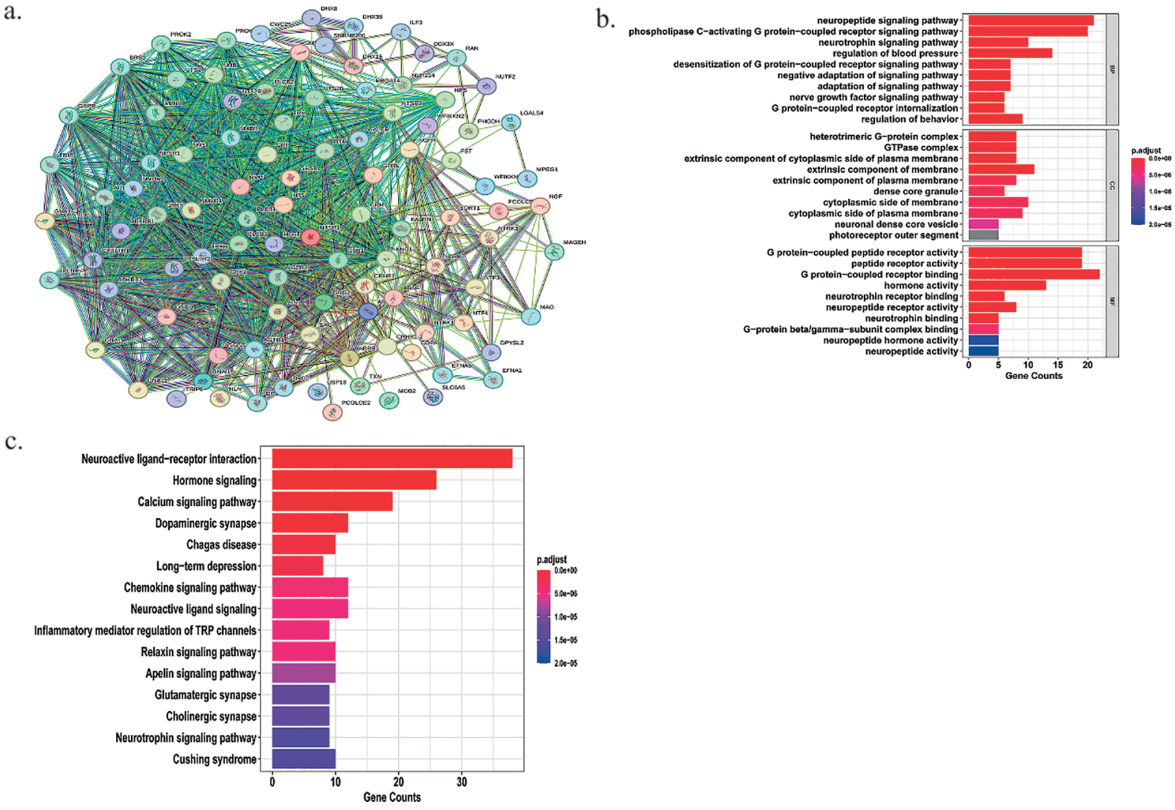

Figure 9. Molecular regulatory mechanism of NTSR1. (a) Adjacent proteins of NTSR1; (b) Potential Biological Functions and Signaling Pathways of NTSR1 in PP: Results from GO Enrichment Analysis; (c) Potential Biological Functions and Signaling Pathways of NTSR1 in PP: KEGG Pathway Enrichment Analysis

3.8 Molecular Docking

The potential active ingredients of FEF were screened by network pharmacology. It was found that eicosapentaenoic acid (EPA) in raw oyster shell *(Ostreae Concha)* and aurantiamide acetate in *Lycium chinensis (Lycii Cortex)* had significant associations with NTSR1. Notably, aurantiamide acetate was detected among the 603 LC-MS-identified ingredients. Molecular docking revealed that the binding energy was −6.9 kcal/mol between kcal and NTSR1, and was −9.5 kcal/mol between aurantiamide acetate and NTSR1,

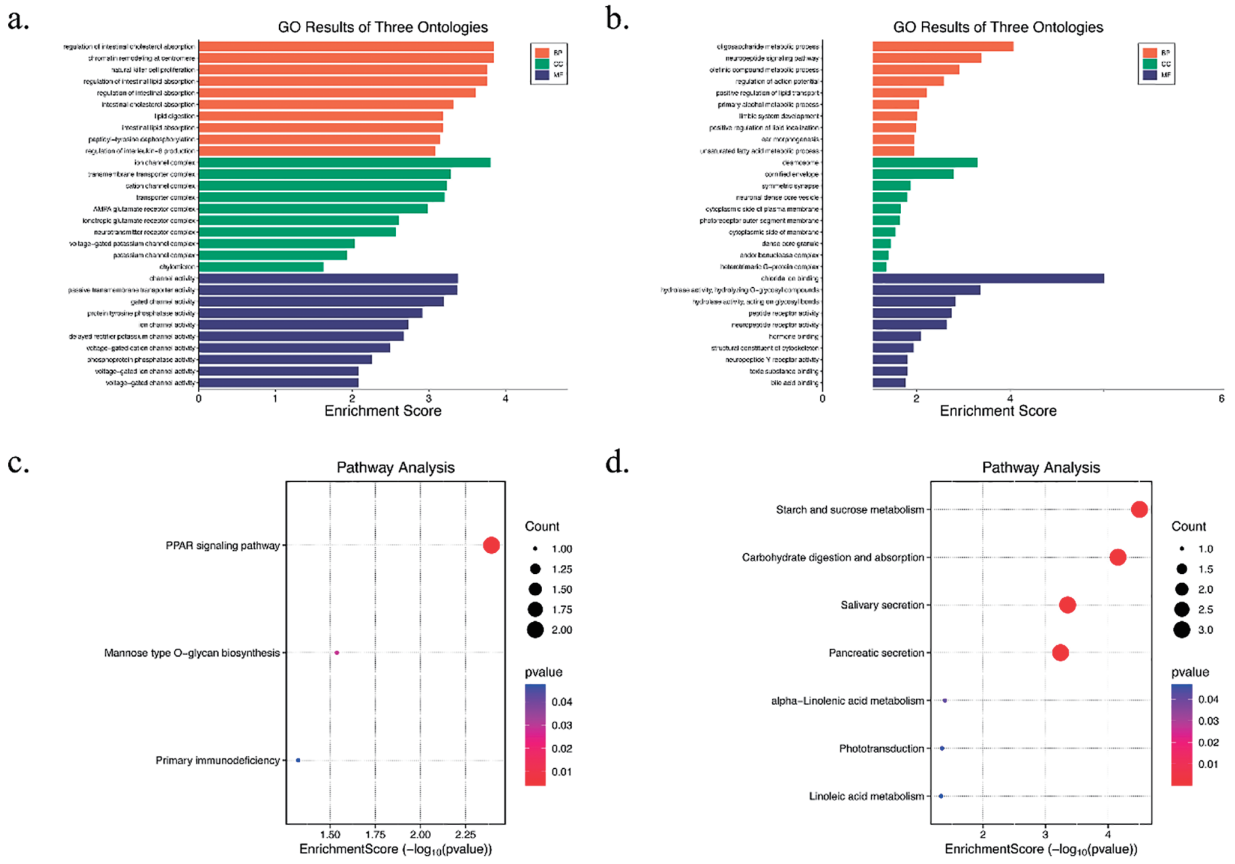

Figure 10. Bidirectional pathway regulation of TCM (CDT) in PP. Separate enrichment analyses of up- and down-regulated DEGs (PP *vs.* CDT groups) showed: up-regulated DEGs enriched in lipid/cholesterol metabolism and immune-related pathways; down-regulated DEGs in glucose metabolism, exocrine function-related, and fatty acid metabolism pathways. (a) Functional enrichment outcomes (GO) associated with the up-regulated genes; (b) Enrichment analysis of KEGG signaling pathways associated with the up-regulated genes; (c) Functional enrichment analysis outcomes (GO) associated with the down-regulated genes; (d) Enrichment analysis of KEGG signaling pathways associated with the down-regulated genes

which were both high-affinity binding (binding energy < −5 kcal/mol). Key interactions included: Aurantiamide acetate formed one hydrogen bond each with LS 250 and GLN 248 of NTSR1 (bond length: 3.6 Å and 3.8 Å), and exhibited hydrophobic interactions with PRO 252, LYS 92, LS 250, and GLN 248. Therefore, LS 250 and GLN 248 were identified as key residues. EPA formed one hydrogen bond with LYS 250 (bond length: 2.7 Å) and exhibited hydrophobic interactions with ARG 182, SER 99, and GLN 248, which were crucial for maintaining stable ligand-receptor binding (Table 4). The strong binding affinity between potential active ingredients and the key target was visualized (Figure 11).

3.9 Effect of FEF on NTSR1 mRNA in Ovarian Tissues of PP Rats

The NTSR1 mRNA expression was far lower in the PP group than in the CON group ($P < 0.01$) and in the HD group ($P < 0.05$) (Figure 12).

4 Discussion

PP is a pediatric endocrine disease, and it causes a significant impact on the children's physical and mental health and family life. Early initiation of HPGA causes the premature secretion of GnRH by the hypothalamus, activates the pituitary gland to release LH and FSH, and activates the gonadal glands to secrete sex hormones (Ministry of Health of the People's Republic of China, 2011). Recently, the incidence of PP has displayed an annually increasing trend, and it is far higher in girls than in boys (Bräuner et al., 2020; Fu et al., 2022).

The chemical ingredients of FEF were systematically examined by UHPLC-MS. A total of 603 potential active ingredients were identified, including naringin, nobiletin, kaempferol, oleic acid, and guanosine. The stability and reproducibility of the detection system were verified via methodological validation, which helps to support the reliability and comparability of the resulting data. The MS analysis clarified the multi-ingredient composition of FEF, which provided a solid guarantee of chemical ingredients

http://doi.org/10.25135/rnp.2510.3665
Rec. Nat. Prod. 2026, 20(2):e25103665

Table 4. Core target binding energy

Target	Protein	Binding energy (kcal/mol)
Aurantiamide_acetate	NTSR1	−9.5
Aurantiamide_acetate	NTSR1	−9.3
Aurantiamide_acetate	NTSR1	−9.2
Aurantiamide_acetate	NTSR1	−9.1
Aurantiamide_acetate	NTSR1	−9.0
Aurantiamide_acetate	NTSR1	−8.7
Aurantiamide_acetate	NTSR1	−8.5
Aurantiamide_acetate	NTSR1	−8.5
Aurantiamide_acetate	NTSR1	−8.4
Aurantiamide_acetate	NTSR1	−8.3
Eicosapentaenoic acid	NTSR1	−6.9
Eicosapentaenoic acid	NTSR1	−6.8
Eicosapentaenoic acid	NTSR1	−6.8
Eicosapentaenoic acid	NTSR1	−6.8
Eicosapentaenoic acid	NTSR1	−6.7
Eicosapentaenoic acid	NTSR1	−6.7
Eicosapentaenoic acid	NTSR1	−6.7
Eicosapentaenoic acid	NTSR1	−6.7
Eicosapentaenoic acid	NTSR1	−6.6
Eicosapentaenoic acid	NTSR1	−6.6

for subsequent pharmacological mechanism research and experimental design.

SD rats, characterized by sensitivity to sex hormones, strong reproductive capacity, rapid growth and development, stable cycles, and compliant character, have been commonly used for PP animal studies (Yu & Zhang, 2023). As revealed by modern studies, the puberty in female rats begins when the vagina opens and the first dioestrus emerges (Huang, 2023). Since the vaginal opening, surrounding tissues, and vaginal exfoliated cells present periodical changes under the regulation of relevant reproductive hormones, the estrous cycle can be determined by observing the vaginal opening status and vaginal exfoliated cell smear in female rats. In this study, PP models were established by NMA subcutaneous injection. It was found that the vagina opened significantly earlier in the PP group, indicating successful modeling. The vaginal exfoliated cell smear can present regular estrous cycles, and a complete estrous cycle contains pro-oestrus, oestrus, meta-oestrus, and dioestrus, during which, regulated by sex hormones, follicular development, rupture, ovulation, and luteinization are completed. We can understand the ovarian and uterine functional status and the levels of sex hormones in female rats by observing the estrous cycle (Zhang et al., 2018; Zhu et al., 2012). In this study, we observed a regular estrous cycle in female rats under the microscope.

Following the onset of puberty, the internal hormonal environment will change, in which GnRH facilitates the LH and FSH secretion by the anterior pituitary gland, thereby contributing to the secretion of sex hormones and gonad development. FSH stimulates the follicular development and enhances the secretion of E2. E2 can enhance the release of FSH and LH via negative feedback, and when reaching its peak during ovulation, it can increase the release of GnRH via positive feedback to sharply increase LH secretion, triggering ovulation and luteinization, and also to enhance the secretion of E2 and progesterone by the corpus luteum (Richter & Lutz, 2016). Therefore, FSH and LH are key hormones for gonadal development and sex hormone secretion, which are implicated in pubertal development and contribute to the maturation of reproductive function (Boegl et al., 2024). In this study, the levels of FSH, LH, E2, and GnRH were far higher in the PP group than in the CON group, while they were far lower in the HD, MD, and triptorelin groups than in the PP group, suggesting that FEF can ameliorate the expression of sex hormones in PP rats, consistent with the effect of the positive control. In terms of gonadal development, the PP group had significantly increased uterine volume and endometrial thickness, an increase in follicles at all levels, and a small number of corpus luteum as compared to the CON group; the HD, MD, and LD groups, especially the HD group, had decreases in the uterine glands, endometrial thickness, and number of corpus luteum and follicles as compared to the PP group.

The ovaries are a pair of vital glands in the female reproductive system, and are responsible for multiple physiological functions primarily involving hormone secretion, oocyte maturation, and ovulation. Therefore, research has been conducted on ovarian tissues. The results of transcriptome sequencing of the ovarian tissues revealed that changes in the mRNA expression of many genes were involved in the pathogenesis of PP and the FEF intervention. We identified four intersecting genes (CYP4F4, PLA2G4C, NTSR1, and OLFM2), and 171 potential active ingredients with 1,332 corresponding targets were retrieved from the database. Then the four genes were intersected with the active ingredient targets to obtain the key target NTSR1. NTSR1 is a G protein-coupled receptor that can be expressed in each part of the HPGA and mediates neurotensin (NT) signaling. The NT/NTSR1 pathway regulates gonadotropin release, and changes in the NTS and NTSR1 expression in the gonadal axis have been observed in the case of early sexual maturation; following administration of NTSR1 antagonists, the levels of FSH and LH significantly rise, indicating that NTSR1 may be a key molecule in the interaction between metabolism and the gonadal axis (González-Gómez et al., 2023; Verma et al., 2024). In this study, RT-qPCR validation was conducted on the key target NTSR1. The NTSR1 expression was far lower in the PP group than in the CON group, and it was far higher in the HD group than in the PP group, displaying great differences. To sum up, NTSR1 acts as a regulator in the ovarian tissues of rats, and FEF can delay PP progression by up-regulating NTSR1.

The PPI analysis was conducted on NTSR1. The GO analysis revealed that the DEGs were primarily enriched in neuropeptide, G protein-coupled receptor, and neurotrophic factor signaling pathways, which were closely related to neuroendocrine regulation. Research suggests that changes in E2 levels can induce the expression of neuropeptides (including NTS) in the AVPV, and directly act on GnRH neurons

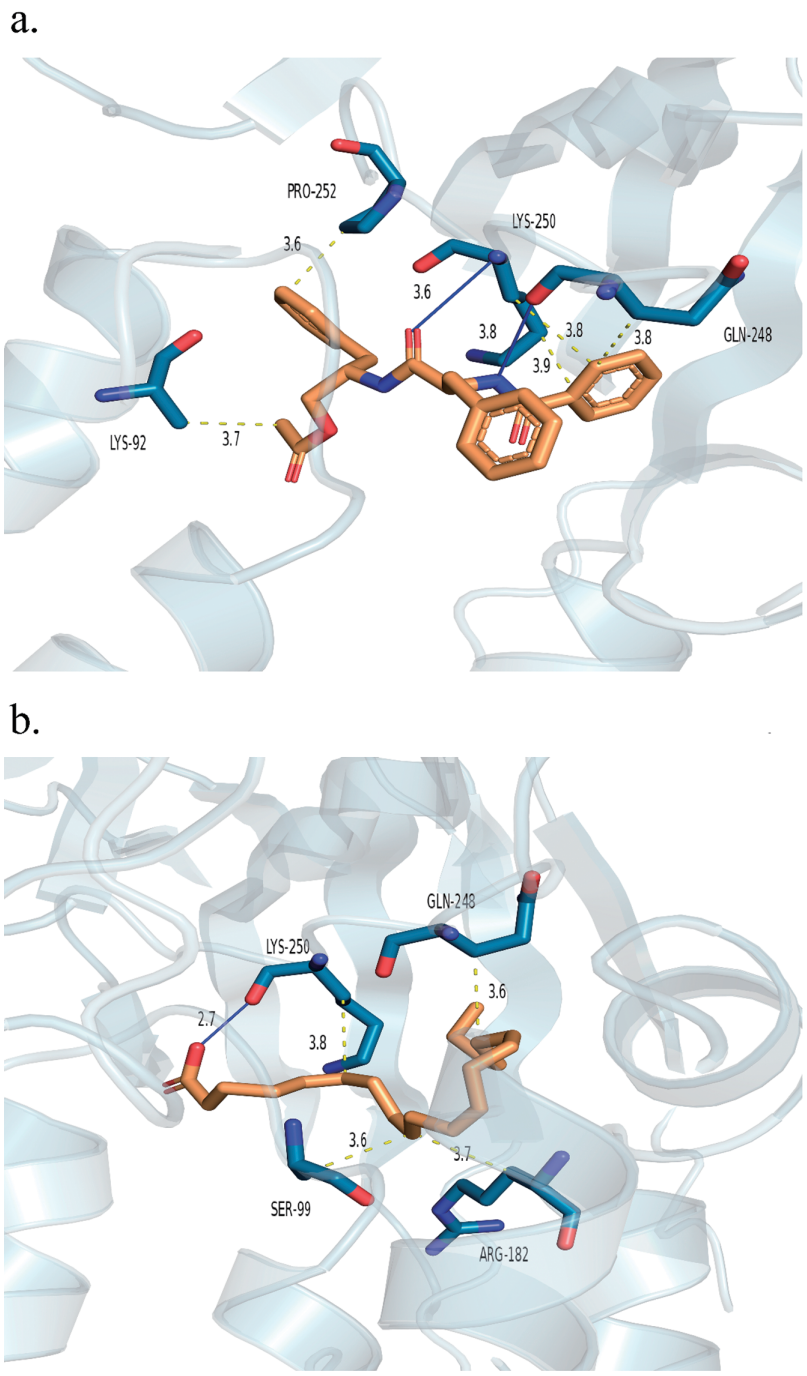

Figure 11. Molecular docking was performed to validate binding activity between NTSR1 and two potential active ingredients: (a) Aurantiamide acetate; (b) Eicosapentaenoic acid

via NTSR1, contributing to GnRH and LH release (Dungan Lemko et al., 2010). The KEGG analysis revealed that the DEGs were mainly enriched in regulating neuroactive ligand-receptor interaction, calcium, and hormone signaling pathways, which were closely related to PP development. It is well known that the neuroactive ligand-receptor interaction covers signaling in neurotransmitters, neuropeptides, and their receptors; in this pathway, the receptors include a variety of G protein-coupled receptors and ion channel receptors, and the ligands include classical neurotransmitters (e.g., norepinephrine, dopamine, and 5-hydroxytryptamine) and neuropeptide modulators, with a wide range of regulatory effect ranging from conduction of neural excitation to endocrine hormone release (Chan et al., 2025). Gonadotroph cells in the anterior pituitary gland can express NT and its receptor NTSR1, which may regulate gonadotropin release by autocrine or paracrine. Calcium signaling is an important player in the onset of puberty. Before puberty, GnRH neurons are in a resting and hypoactive state, which is largely attributed to their ion channel activity and the

http://doi.org/10.25135/rnp.2510.3665
Rec. Nat. Prod. 2026, 20(2):e25103665

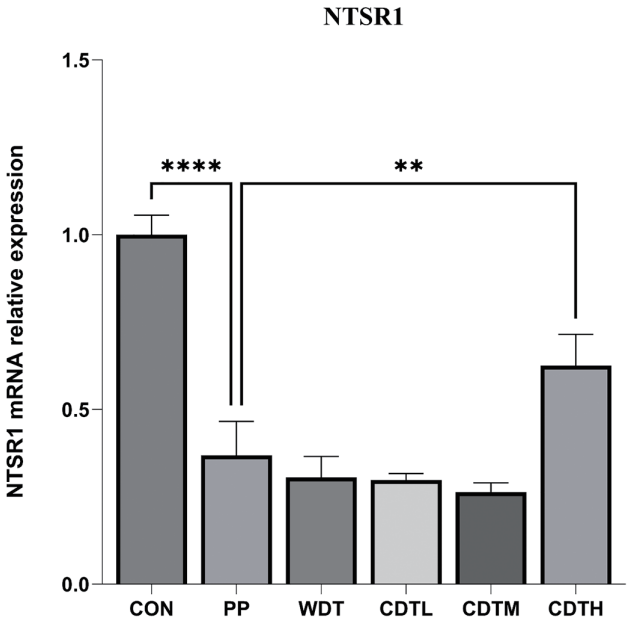

Figure 12. Effect of FEF on NTSR1 mRNA in ovarian tissues of PP rats

development status of the inhibitory neural pathway. After entering puberty, both discharge frequency and amplitude of GnRH neurons rise, accompanied by an increase in intracellular Ca^{2+} channel events (Jaime & Moenter, 2022). On this basis, common trends were found between the results of NTSR1 interacting protein enrichment analysis and DEG enrichment analysis. NTSR1 neuropeptide signaling may not solely regulate neural activity but reshape metabolic patterns through GPCR signaling networks, which redirects cellular nutrition utilization toward lipid and cholesterol uptake and processing, thereby establishing metabolic reprogramming characterized by a "shift from glucose metabolism to lipid metabolism". Notably, the up-regulated DEGs were significantly enriched in pathways related to natural killer cell proliferation and IL-8. NTSR1 interacting proteins were enriched in immune/inflammation-related pathways such as chemokine signalling pathway and inflammatory mediator regulation of TRP channels. This longitudinal correlation suggests that NTSR1-mediated neuropeptide signaling may regulate metabolic remodeling and tightly couple neuroendocrine signaling with immune responses *via* modulation of chemokines and inflammatory mediators. To sum up, NTSR1 may be an important regulator linking energy metabolism and inflammatory responses. Molecular docking between EPA and aurantiamide acetate and NTSR1 indicated that EPA and aurantiamide acetate exhibited favorable docking with NTSR1, confirming that FEF may regulate synaptic plasticity through these targets.

5 Conclusion

FEF contains a variety of pharmacologically active ingredients, which can delay the development of the uterus and ovary, and ameliorate the expression of FSH, LH, E2, and GnRH in female rats with PP. We analyzed the potential active ingredients, target genes, and molecular signaling pathways of FEF by transcriptomics and network analysis, and identified the key target NTSR1. The preliminary findings suggest that FEF delays PP progression via the neuroactive ligand-receptor interaction, calcium, G protein-coupled receptor, and hormone signaling pathways. The main limitations of this study are as follows: 1) The standardized decoction procedure was lacking. Large-scale standardized decoction followed by freeze-drying of extracts is needed in the future to enhance experimental reproducibility. 2) No quantitative analysis was conducted on the pharmaceutical extracts within the scope of the present study. In subsequent research endeavors, quantitative analysis will be performed in strict compliance with relevant standard protocols. 3) FEF has complex ingredients and various targets, and the sample size of transcriptomics was small, so its mechanism failed to be fully summarized. In the future, *in vitro* and *in vivo* experiments and validation are further required for the relevant mechanisms, thereby guiding the exploration of new PP treatment strategies.

Funding Statement

This study was supported by National Famous Traditional Chinese Medicine Experts Inheritance Studio Construction Project (National Chinese Medicine Education letter (2022) No. 75).

Author Contributions

Yanli Wang: Conceptualization, Methodology, Software, Validation, Data Curation, Writing—Original Draft, Writing—Review & Editing; Hao Liu: Formal analysis, Writing—Review & Editing; Lili Zhang: Validation, Supervision, Writing—Review & Editing; Wen Tang: Validation, Investigation, Writing—Review & Editing; Han Jiang: Investigation, Writing—Review & Editing; Lei Gu: Investigation, Writing—Review & Editing; Sijie Fan: Validation, Writing—Review & Editing; Yimin Li: Validation, Writing—Review & Editing; Xi Wang: Validation, Writing—Review & Editing; Lili Shang: Resources, Visualization, Data Curation, Writing—Review & Editing, Project administration, Funding acquisition.

Availability of Data and Materials

The authors declare that the data supporting the findings of this study are available within the paper and its Supplementary Information files. Should any raw data files be needed in another format they are available from the corresponding author upon reasonable request. Source data are provided with this paper.

Ethics Approval

The Ethics Committee of the First Affiliated Hospital of Anhui University of Chinese Medicine approved all animal

experiments (approval No.: AZYFY-2025-1013), in compliance with the National Institutes of Health guidelines for the care and use of laboratory animals.

Conflicts of Interest

The authors declare that they have no known competing financial interests or personal relationships that could have appeared to influence the work reported in this paper.

Supporting Information

Supporting Information accompanies this paper on http://www.acgpubs.org/journal/records-of-natural-products.

ORCID

Yanli Wang: 0009-0001-6802-4573
Hao Liu: 0009-0007-1592-2373
Lili Zhang: 0009-0005-1203-2346
Wen Tang: 0009-0005-0415-7341
Han Jiang: 0009-0008-5699-9841
Lei Gu: 0009-0007-1637-062X
Sijie Fan: 0009-0005-4743-2251
Yimin Li: 0009-0008-4602-2041
Xi Wang: 0009-0000-3931-7775
Lili Shang: 0009-0009-5131-3561

References

Boegl, M., Dewailly, D., Marculescu, R., Steininger, J., Ott, J. & Hager, M. (2024). The LH:FSH ratio in functional hypothalamic amenorrhea: An observational study. *Journal of Clinical Medicine*, *13*(5), 1201–1212. DOI: 10.3390/jcm13051201.

Bräuner, E. V., Busch, A. S., Eckert-Lind, C., Koch, T., Hickey, M. & Juul, A. (2020). Trends in the incidence of central precocious puberty and normal variant puberty among children in Denmark, 1998 to 2017. *JAMA Network Open*, *3*(10), e2015665. DOI: 10.1001/jamanetworkopen.2020.15665.

Chan, R. J., Walker, A., Vardy, J., Chan, A., Oppegaard, K., Conley, Y. P., Paul, S. M., Kober, K. M., Harris, C., Shin, J., Morse, L., Roy, R., Olshen, A., Hammer, M. J., Levine, J. D. & Miaskowski, C. (2025). Perturbations in the neuroactive ligand-receptor interaction and renin angiotensin system pathways are associated with cancer-related cognitive impairment. *Supportive Care in Cancer*, *33*(4), 254. DOI: 10.1007/s00520-025-09317-9.

Dong, B., Zhi, M., Han, M., Yu, H., Lin, H. & Li, L. (2020). Early menarche is associated with insulin resistance in advanced maternal age before delivery. *Gynecological Endocrinology*, *36*(4), 341–345. DOI: 10.1080/09513590.2019.1658731.

Doppler, M., Kluger, B., Bueschl, C., Schneider, C., Krska, R., Delcambre, S., Hiller, K., Lemmens, M. & Schuhmacher, R. (2016). Stable isotope-assisted evaluation of different extraction solvents for untargeted metabolomics of plants. *International Journal of Molecular Sciences*, *17*(7), 1017. DOI: 10.3390/ijms17071017.

Dungan Lemko, H. M., Naderi, R., Adjan, V., Jennes, L. H., Navarro, V. M., Clifton, D. K. & Steiner, R. A. (2010). Interactions between neurotensin and GnRH neurons in the positive feedback control of GnRH/LH secretion in the mouse. *American Journal of Physiology-Endocrinology and Metabolism*, *298*(1), E80–88. DOI: 10.1152/ajpendo.00380.2009.

Fu, D., Li, T., Zhang, Y., Wang, H., Wu, X., Chen, Y., Cao, B. & Wei, H. (2022). Analysis of the incidence and risk factors of precocious puberty in girls during the COVID-19 pandemic. *International Journal of Endocrinology*, *2022*(53), 9229153. DOI: 10.1155/2022/9229153.

González-Gómez, M., Reyes, R., Damas-Hernández, M. D. C., Plasencia-Cruz, X., González-Marrero, I., Alonso, R. & Bello, A. R. (2023). NTS, NTSR1 and ERs in the pituitary-gonadal axis of cycling and postnatal female rats after BPA treatment. *International Journal of Molecular Sciences*, *24*(8), 7418–7443. DOI: 10.3390/ijms24087418.

He, L. (2023). *Mechanism of Jiuwei Chushi Granules for Treating Precocious Puberty: Based on Network Pharmacology and Molecular Docking*. Wuhan: Hubei University of Chinese Medicine.

Huang, T. (2023). *Effects and Mechanism of Jiuwei Chushi Formula on Female CPP Model Rats: Based on SIRT1/Kiss-1 Signaling Pathway*. Wuhan: Hubei University of Chinese Medicine.

Huang, W., Masureel, M., Qu, Q., Janetzko, J., Inoue, A., Kato, H. E., Robertson, M. J., Nguyen, K. C., Glenn, J. S., Skiniotis, G. & Kobilka, B. K. (2020). Structure of the neurotensin receptor 1 in complex with β-arrestin 1. *Nature*, *579*(7798), 303–308. DOI: 10.1038/s41586-020-1953-1.

Jaime, J., & Moenter, S. M. (2022). GnRH neuron excitability and action potential properties change with development but are not affected by prenatal androgen exposure. *eNeuro*, *9*(6), ENEURO.0362-22.2022. DOI: 10.1523/eneuro.0362-22.2022.

Jiang, M., Gao, Y., Wang, K. & Huang, L. (2023). Lipid profile in girls with precocious puberty: A systematic review and meta-analysis. *BMC Endocrine Disorders*, *23*(1), 225. DOI: 10.1186/s12902-023-01470-8.

Ministry of Health of the People's Republic of China. (2011). Guidelines for diagnosis and treatment of precocious puberty (trial) [Document No.: Medical Administration Office (195)]. *Chinese Journal of Child Health Care*, *19*(4), 390–392. Retrieved from https://d.wanfangdata.com.cn/periodical/zgetbjzz201104035.

Park, S. C., Trinh, T. A., Lee, W. Y., Baek, J. Y., Lee, S., Choi, K., Ha, J., Kim, C. E., Kang, K. S. & Lee, H. L. (2021). Effects of estrogen inhibition formula herbal mixture for danazol-induced precocious puberty in female rats: an experimental study with network pharmacology. *Integrative Medicine Research*, *10*(3), 100708. DOI: 10.1016/j.imr.2020.100708.

Richter, D., & Lutz, T. A. (2016). Feedback regulation of gonadotropin secretion and reproductive function. *Endocrine Reviews*, *37*(5), 565–595.

Sumner, L. W., Amberg, A., Barrett, D., Beale, M. H., Beger, R., Daykin, C. A., Fan, T. W.-M., Fiehn, O., Goodacre, R., Griffin, J. L., Hankemeier, T., Hardy, N., Harnly, J., Higashi, R., Kopka, J., Lane, A. N., Lindon, J. C., Marriott, P., Nicholls, A. W., Reily, M. D. et al. (2007). Proposed minimum reporting standards for chemical analysis. *Metabolomics*, *3*(3), 211–221. DOI: 10.1007/s11306-007-0082-2.

Umano, G. R., Maddaluno, I., Riccio, S., Lanzaro, F., Antignani, R., Giuliano, M., Luongo, C., Festa, A., Miraglia Del Giudice, E. & Grandone, A. (2022). Central precocious puberty during COVID-19 pandemic and sleep disturbance: An exploratory study. *Italian Journal of Pediatrics*, *48*(1), 60. DOI: 10.1186/s13052-022-01256-z.

Verma, P., Pal, H. & Mohanty, B. (2024). Neurotensin receptor-1 antagonist SR48692 modulation of high-fat diet induced reproductive impairment in male mice. *Reproductive Toxicology*, *123*(2), 108498. DOI: 10.1016/j.reprotox.2023.108498.

Wang, J., Zhang, T., Shen, X., Liu, J., Zhao, D., Sun, Y., Wang, L., Liu, Y., Gong, X., Liu, Y., Zhu, Z.-J. & Xue, F. (2016). Serum metabolomics for early diagnosis of esophageal squamous cell carcinoma by UHPLC-QTOF/MS. *Metabolomics*, *12*(7), 116. DOI: 10.1007/s11306-016-1050-5.

Wei, W., Wu, X. & Li, Y. (2010). *Experimental Methodology of Pharmacology*. 4th ed. Beijing: People's Medical Publishing House.

Wu, W., Zhu, X., Chen, Y., Yang, X., Zhang, Y. & Chen, R. (2023). Development and validation of a model for predicting the adult height of girls with idiopathic central precocious puberty. *European Journal of Pediatrics*, *182*(4), 1627–1635. DOI: 10.1007/s00431-023-04842-3.

Xiong, Y., Cheng, M. & Xu, K. (2023). Interpretation of the expert consensus on the diagnosis and treatment of central precocious puberty. *2022 Journal of Practical Obstetrics and Gynecology*, *39*(06), 422–424. DOI: 10.3969/j.issn.1003-6946.2023.6.syfckzz202306008.

Yang, H., Luo, S. Q., Tang, F., Zeng, L., Cheng, T., Zhu, M., Lin, Q., Liang, X. H. & Wu, D. M. Q. X. (2020). Study on the quality of life of children with precocious puberty and its influence factors. *Chinese Nursing Management*, *20*(12), 1795–1800. DOI: 10.3969/j.issn.1672-1756.2020.12.009.

Yu, J., Sun, W. & Sun, Y. (2024). Guideline for the diagnosis and treatment of precocious puberty in children with integrated traditional Chinese and western medicine (2023 edition). *Journal of Traditional Chinese Medicine*, *65*(05), 546–552.

Yu, S. W. J., Zhang, G. (2023). Advances in animal modeling of precocious puberty. *Acta Laboratorium Animalis Scientia Sinica*, *31*(02), 265–278. DOI: 10.3969/j.issn.1005-4847.2023.02.017.

Zevin, E. L., & Eugster, E. A. (2023). Central precocious puberty: a review of diagnosis, treatment, and outcomes. *The Lancet Child & Adolescent Health*, *7*(12), 886–896. DOI: 10.1016/s2352-4642(23)00237-7.

Zhang, T., Wang, Y. & Wang, L. (2018). Comparison of two staining methods for rat vaginal smears. *Chinese Journal of Comparative Medicine*, *28*(12), 98–101. DOI: 10.3969/j.issn.1671-7856.2018.12.016.

Zhang, X. (2020). *Analysis of Cognitive and Psychological Development Status and Influencing Factors in Girls with Idiopathic Central Precocious Puberty*. Zhengzhou: Zhengzhou University.

Zhou, Z., Luo, M., Zhang, H., Yin, Y., Cai, Y. & Zhu, Z. J. (2022). Metabolite annotation from knowns to unknowns through knowledge-guided multi-layer metabolic networking. *Nature Communications*, *13*(1), 6656. DOI: 10.1038/s41467-022-34537-6.

Zhu, N., Jia, H. X., Liu, X. K., Zhao, X. E., Wei, Q. & Ma, B. H. (2012). [Measuring the estrus cycle and its effect on superovulation in mice]. *Dongwuxue Yanjiu*, *33*(3), 276–282. DOI: 10.3724/sp.J.1141.2012.03276.